Construction and Building Materials 411 (2024) 134588

Contents lists available at ScienceDirect

Construction and Building Materials

journal homepage: www.elsevier.com/locate/conbuildmat

Corrosive effect of HCl and H_2SO_4 exposure on the strength and microstructure of lithium slag geopolymer mortars

Usman Javed *, Faiz Uddin Ahmed Shaikh *, Prabir Kumar Sarker

School of Civil and Mechanical Engineering, Curtin University, Perth, Australia

ARTICLE INFO

Keywords:
Aggressive effects
Lithium slag geopolymer
Residual strength
Calorimetric heat evolution
Microstructure
Degradation

ABSTRACT

Resistance of geopolymer against aggressive effects of strong acid governs its service life. This research investigates the effect of silica fume incorporation on the strength degradation of lithium slag geopolymer (LSG) mortars after exposure to strong acids and presents the relationship between microstructure, calorimetry, and residual strength. Silica fume incorporated LSG mortars containing sodium (Na) and potassium (K) based alkaline activators were exposed to 5% sulphuric and hydrochloric acid solutions separately for 60 days. The sulphuric acid deterioration of LSG in terms of maximum percentage reduction in compressive strength was 37.42% upon incorporating 40% silica fume in geopolymer with a Na-based alkaline activator. LSG mixes activated by Na-activators demonstrated higher acid resistance compared to those activated by K-based activators. Leaching of aluminium (Al) from the aluminosilicate gel matrix occurred, which subsequently deteriorated aluminosilicate gel matrix when exposed to hydrochloric acid, whereas the leaching of Al occurs alongside the crystallization of calcium sulfate when specimens were exposed to sulphuric acid solution. The incorporation of silica fume reduces the initial calorimetric heat evolution and higher degree of geopolymerization marked by higher heat evolution between 5–48 h than the control LSG. The intense evolution of heat in control LSG at the initial stage of geopolymerization yielded a poor microstructure. Thus, acid-induced strength degradation is lower in silica fume-incorporated gel due to its denser microstructure and higher quantity of aluminosilicate gel formation. Hence, the incorporation of silica fume significantly improved its acid resistance, thus LSG may have industrial applications concerning acid exposure.

1. Introduction

The demand for environmentally friendly construction materials has led to a notable increase in research efforts focused on developing geopolymers. The growing demand for cement has raised environmental concerns for researchers as conventional cement production evolves approximately 4 billion tons of carbon emission annually (as reported in 2012) which is equivalent to that of cement production [1]. Half part of the carbon emissions is contributed by the calcination of calcium carbonate and the rest half toward the production of cement [2]. The concentration of carbon footprints in the atmosphere is drastically increasing with the projection from 380 ppm by now to 800 ppm by the end of this century [3,4]. Unlike cement, the formation of geopolymer constituents i.e. solid precursor and alkaline activator do not evolve carbon footprints of such a higher extent [5]. Whereas, alkali-activated materials can provide up to 80% reduction in greenhouse emissions compared to that of cement [6]. The environmental concern regarding the significant carbon emissions associated with cement production has prompted efforts to decrease the production of clinker-based cement and use low-carbon binders while continuing to fulfill the demands of the construction industry. While comparing with clinker cement, geopolymer binders release lower carbon emissions cumulatively during the manufacturing of their constituents and the geopolymer production. Geopolymerization is a chemical process involved in strength development wherein aluminosilicate minerals and alkaline activators undergo a reaction to produce an inorganic amorphous material called

Abbreviation: HCl, Hydrochloric acid; H_2SO_4, Sulphuric acid; LSG, Lithium Slag Geopolymer; Na, Sodium; K, Potassium; Al, Aluminium; SEM, Scanning Electron Microscopy; EDS, Energy Dispersive X-ray Spectroscopy; K_2O, Potassium Oxide; TIMA, TESCAN Integrated Mineral Analyzer; Si/Al, Silica to alumina ratio; ASTM, American Society for Testing and Materials; N-C-A-S-H, Sodium (calcium) Aluminosilicate Hydrate; LSG_{Na}, Lithium Slag Geopolymer containing sodium based alkaline activators; LSG_K, Lithium Slag Geopolymer containing potassium based alkaline activators.

* Corresponding authors.
E-mail addresses: usman.javed1@postgrad.curtin.edu.au (U. Javed), s.ahmed@curtin.edu.au (F.U.A. Shaikh).

https://doi.org/10.1016/j.conbuildmat.2023.134588
Received 7 September 2023; Received in revised form 29 November 2023; Accepted 11 December 2023
Available online 19 December 2023

Table 1
Chemical composition of calcined lithium slag, silica fume, and fly ash [33].

Oxides	SiO_2	Al_2O_3	Fe_2O_3	CaO	MgO	MnO	TiO_2	SO_3	P_2O_5	K_2O	Na_2O	LOI
Lithium slag	54.53	21.08	1.45	7.53	0.57	0.23	0.05	5.62	0.48	0.88	0.72	6.76
Silica Fume	94.58	0.50	0.06	1.54	0.41	-	-	0.14	0.11	0.64	0.23	1.79

geopolymer. Geopolymer is an inorganic amorphous material that is synthesized by a chemical reaction between aluminosilicate minerals and alkaline activators, widely known as geopolymerization [7]. It has the potential to serve as an eco-friendly substitute for conventional cement. It has potential benefits, including a higher strength, lower energy requirements, and carbon dioxide emissions associated with it [8]. There are various aluminosilicate-rich precursors such as fly ash [9], metakaolin [10], blast furnace slag[11], ferronickel slag [12], and

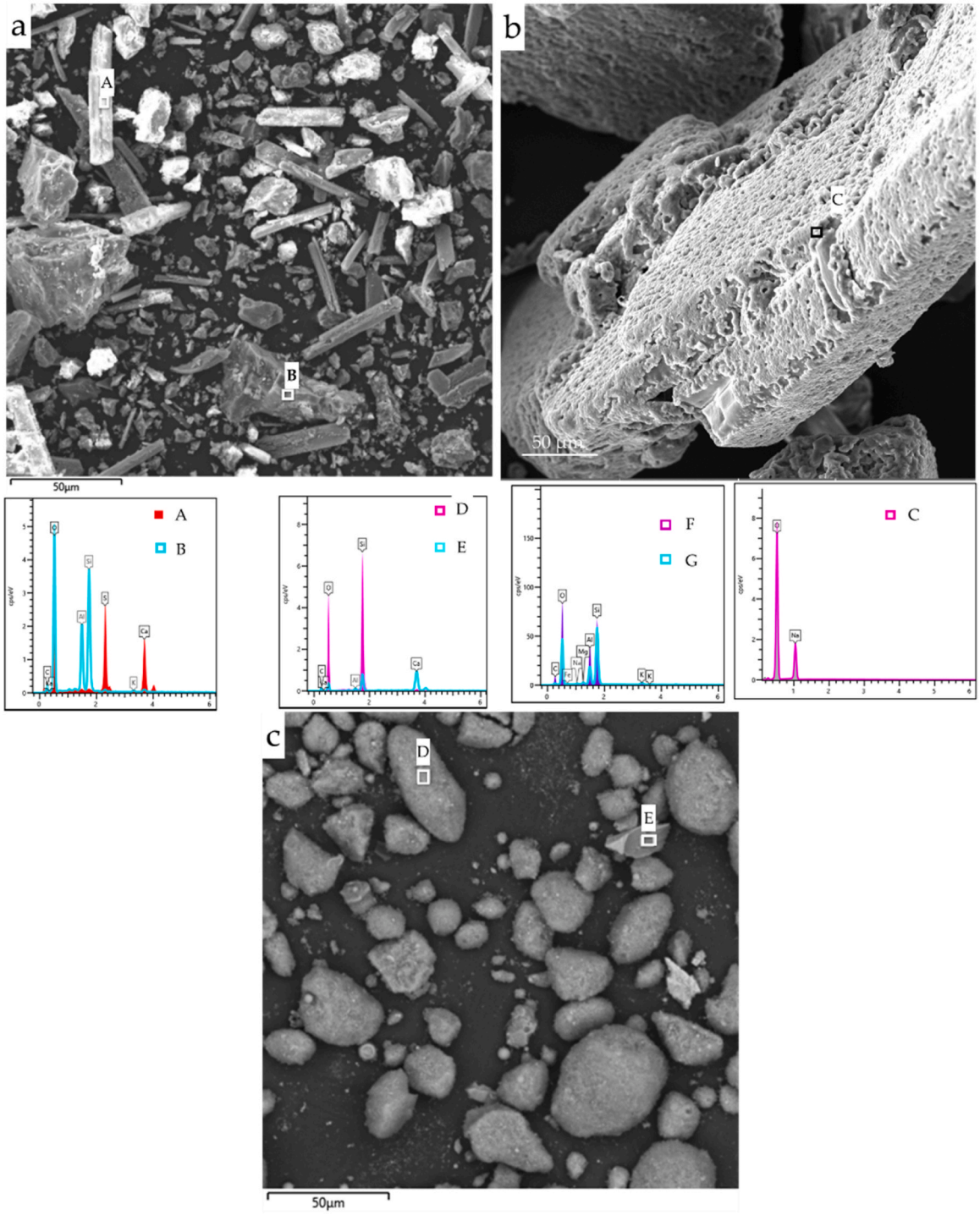

Fig. 1. Micro-morphology and EDS spectra a) lithium slag [33] b) Sodium tetraborate [37] c) Densified silica fume [37].

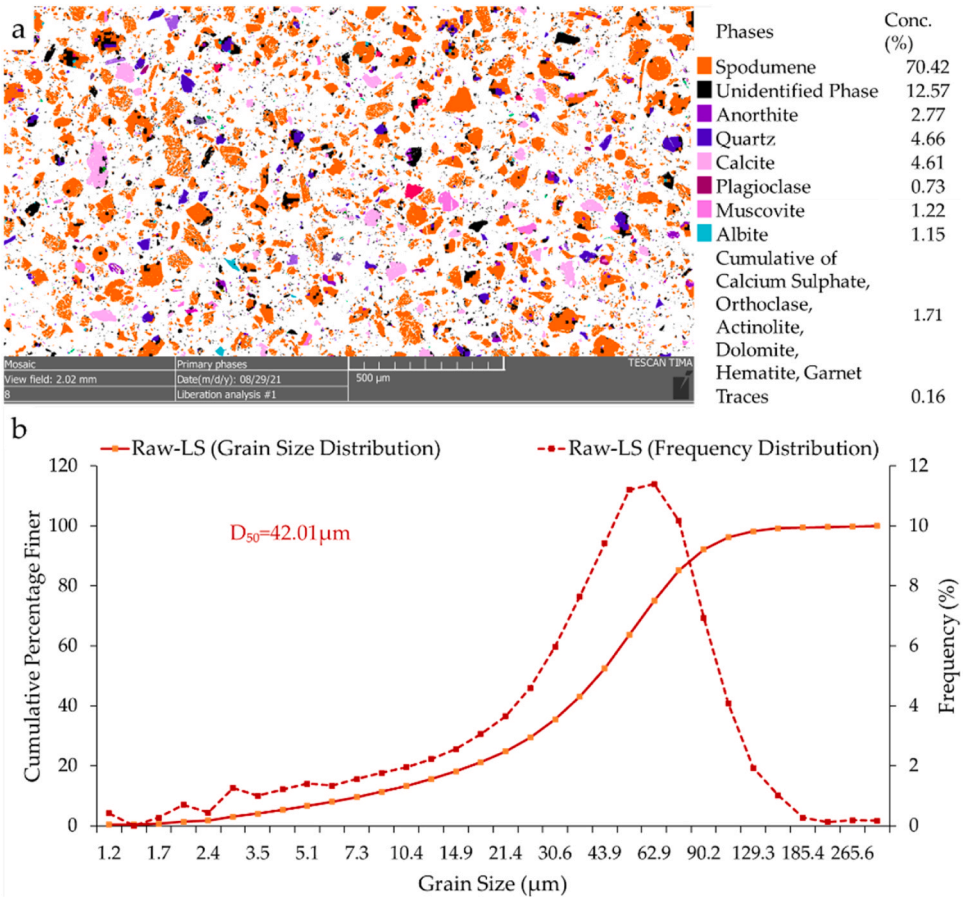

Fig. 2. Particle characterization of raw lithium slag a) Mineral composition and b) Automated particle size distribution performed by TESCAN TIMA [33,38].

lithium slag used in geopolymer with lower carbon footprints associated with the clinker-based cement concrete [13]. Nowadays, lithium slag is one of the emerging mining slags due to the increasing extraction of lithium for energy storage in electric vehicles, space exploration, and electronics [14].

The process of geopolymerization involves exothermic reaction with the complex molecular interactions and formation of bonding among O-Si-O and O-Al-O monomers, imparting geopolymer higher mechanical properties. The degree of geopolymerization and strength development mechanism is often addressed by studying its reaction kinetics using various techniques such as isothermal calorimetry [15]. Isothermal calorimetry is widely used to capture the early-stage dynamic variation of heat release during geopolymerization and provides valuable insights into reaction kinetics. The dissolution of aluminosilicate minerals and the formation of silicate and aluminate monomers are associated with the first calorimetric peak [16,17]. The strength development of geopolymer formation of long-chained aluminosilicate gel corresponds to the heat evolved during the deceleration stage of calorimetric peak [17,18].

The durability of geopolymers is an important factor affecting the design life of a structure [19], and the durable geopolymer could minimize the maintenance and concrete disposal waste, thereby reducing the associated carbon footprints. Strong acids, such as sulphuric acid, hydrochloric acid, and nitric acid, found in acid rain and industrial effluents [20], can deteriorate the geopolymer paste matrix because of its alkaline composition. Exposure to an acidic environment can dissolve the binder phase, leach alkali cations, weaken the microstructure, and reduces the mechanical strength [21]. Synthesizing geopolymers with higher durability would not only resolve the issues related to sustainability but also expand their potential applications in sectors where resistance to acids is a critical requirement such as in industrial applications.

Activated materials and concrete are susceptible to damage in acidic environments because of their caustic properties. During the service life of a structure, it may come into contact with highly corrosive acids such as nitric acid, hydrochloric acid, and sulfatic environments from complex soil, industrial waste, and marine conditions during structure operation [22–24]. One of the major durability concerns to geopolymers is sulfate attack which occurs upon exposure of the structure to the sulphatic environment such as contaminated soil, groundwater, marine environment, or wastewater treatment infrastructure [25–29]. The severity of a sulphate attack depends on the geochemistry of the geopolymer paste matrix, concrete quality, and moisture resistance. Sulphate ions react more with calcium hydroxide and aluminum-containing species to form expansive products like ettringite and gypsum which damage geopolymer pore structure. The deterioration of geopolymer exposed to aggressive acidic environments such as in industrial activities governs the service life of geopolymer. The deterioration effect of acid exposure is also dependent on the reaction kinetics and strength development rate of the geopolymer [30,31]. This research investigates the accelerated deterioration of LSG containing silica fume caused by strong acids such as H_2SO_4 and HCl and the deterioration was gauged by residual strength and weight loss due to the corrosive action of acids. Micro-forensic analysis was conducted on LSG after the acid exposure using Scanning Electron Microscopy (SEM) and Energy Dispersive X-ray Spectroscopy (EDS) to examine the extent of chemical and morphological deterioration in the microstructure that has caused strength degradation. As the rate of strength development affects the microstructure evolution, therefore the reaction kinetics of LSG geopolymer was also studied by conducting calorimetry and correlated its results with

residual strength. Conclusively, this study comprehensively investigates the effect of silica fume incorporation on strength degradation upon exposure to strong acids and presents the relationship among microstructure, calorimetry, and residual strength.

2. Materials and methods

2.1. Materials

Lithium slag is the aluminosilicate-rich mineral used for synthesizing geopolymer. Sodium tetraborate was used as retarder. Before using lithium slag, it was calcined at 700°C followed by grinding for half an hour. Densified silica fume (15–30 m^2/kg specific area) was used as an additive in LS-geopolymer supplied by Ecotec Australia [32]. Sodium and potassium-based alkaline activators were used in geopolymer supplied by Rowe Scientific and PQ Australia.

Chemical oxide compositions of lithium slag and silica fume are shown in Table 1. Borax (sodium tetraborate) was employed to delay the rapid setting of silica fume-added geopolymer. The sodium hydroxide and potassium hydroxide solution had a molarity of 10 M, and sodium silicate (specific gravity: 1.53 g/cm^3) contained Na_2O, SiO_2, and water in proportions of 14.70%, 29.40%, and 55.90%, respectively. Potassium silicate had a concentration of K2O, SiO2, and water content of 11.2%, 24.8%, and 64%, respectively. The acid resistance of the geopolymer was determined using 32% concentrated HCl and 98% concentrated H_2SO_4 supplied by Chem-supply and Merck, respectively.

2.2. Characterization

In the authors' previous studies [33,34], lithium slag was characterized by various characterization techniques such as laser-diffraction particle size distribution analysis, scanning electron microscopy with energy dispersive spectroscopy, X-ray fluorescence, and X-ray diffraction to determine the particle size distribution, micromorphology, chemical, crystallographic, and mineral phase compositions of calcined lithium slag.

The morphology and EDS spectra of lithium slag, sodium tetraborate, and densified silica fume is presented in Fig. 1. SEM/EDS analysis shows that the angular particles in lithium slag are rich in alumino-silicate minerals (Fig. 2-a), while the prismatic/elongated particles are made of gypsum. Peaks in the aluminum, silicon, and oxygen EDS spectra can be seen at B and C on the micrograph, indicating the presence of aluminosilicate particles. Sulphation upon lithium extraction in refineries can be demonstrated through the EDS of prismatic particles, which showed an increase in the intensity of calcium, sulfur, and oxygen, indicating the presence of gypsum [35]. Prism-shaped particles have a size greater than 50 μm. The relative Li content, which is a key factor for the durability resistance of geopolymer, was measured by TIMA based on EDS spectral data and the obtained value for Li was 2.15% by weight. This technique is considered to be sufficiently accurate for estimating the Li content in the sample comparative to absolute analytical methods such as Induced Couple Plasma Mass Spectroscopy (ICPMS) [36].

According to the Rietveld refinement results presented in authors' previous research [33], the lithium slag is primarily composed of spodumene, anorthite, quartz, calcite, and anhydrite, with 84% content of the amorphous phase. Fig. 2 displays the results of a laser particle size analysis of lithium slag, which show that the particle size ranges from 280 nm to 470 μm, with an average particle size of 43.15 μm.

2.3. Mix Proportions

The LSG specimens were prepared by replacing 0%, 10%, 20%, 30%, and 40% of lithium slag with silica fume. The geopolymer specimens were prepared for both sodium and potassium-based alkaline activators by adding 3% sodium tetraborate to LSG to avoid the flash setting of the geopolymer matrix [34,39]. The ratio of alkali silicate to alkali hydroxide was 3, while the molarity of alkali (Na, K) hydroxide was kept at 10 M. The alkaline activator solution used in developing geopolymer was 50% weight of aluminosilicate precursor. The net Si/Al ratio of geopolymer increased from 2.62 to 5.55 in LSG considering silica content in the form of aluminosilicate and additive silica fume, while only considering additive silica fume the Si/Al ratios were between 0 to 2.92.

2.4. Synthesizing geopolymer

The geopolymer mortar was prepared through a process involving the dry blending of lithium slag, silica fume, and sodium tetraborate in a Hobart mixer for a duration of 30 s. Subsequently, the mixture was further mixed for one minute after the addition of the alkaline activator solution. For dry mixing the mixing speed was kept at 116 rpm, whereas the mixing speed was 380 rpm for wet mixing. Silica fume additive LSG fresh mortar was placed in acrylic cubes of size 50×50×50 mm^3. Thereafter, the geopolymer was compacted on the vibration table for one minute and the ambient curing was adopted due to the presence of silica fume in the mix for better strength gain as reported in the literature [33]. The freshly cast specimens were placed in ambient curing at 25°C and at a relative humidity of 95% as per ASTM 511–21 [40], and the specimens were tested at their desired curing age.

2.5. Experimental program

2.5.1. Acid exposure

The resistance to the corrosive effect of inorganic acids such as H_2SO_4 and HCl was assessed using an accelerated method, which followed the guidelines outlined in ASTM C267 [41]. The investigation focused on the strength loss and mass loss of mortar samples prepared using both sodium and potassium-based alkaline activators. Specimens of LSG mortar, sized 50×50×50 mm^3, were immersed in 5% v/v solutions of HCl and H_2SO_4 for 60 days, after having been cured for 28 days. Sets of four cubes from each mix were then placed in High-Density Polyethylene (HDPE) boxes containing acid solutions with a concentration of 5% by volume. A key challenge for geopolymer applications is the long-term durability resistance of the material under environmental conditions. To assess the corrosion resistance of geopolymer over extended periods of time, accelerated tests using strong acids such as HCl and H_2SO_4 were conducted. The acid solutions were subject to dilution over time as a result of the leaching reaction. To maintain the molarity of the solutions at approximately 0.919 M and 0.609 M for H_2SO_4 and HCl, respectively (equivalent 5% v/v solution), the acid concentrations were adjusted every 15 days by acid-base titration. The titration used sodium hydroxide as the base and phenolphthalein as the indicator, and the molarity of the corrosive solution was calculated using the following equation:

Moles of H^+=Moles of OH^- at equivalence point.

$M_A \times V_A = n\ M_B \times V_B$.

n: Coefficient of acids (2 for H_2SO_4 and 1 for HCl).

M_A is acid molarity, V_A is acid volume, M_B is base molarity, and V_B is base volume. The factor of 2 is because sulfuric acid is diprotic and donates two protons per molecule.

The acidic solutions were replenished after every 15 days to maintain the molarity of the solutions. Thereafter, the specimens were then tested for strength degradation and weight loss. The fractured specimens from the middle were prepared for SEM/EDS analysis.

2.5.2. Compressive strength

The compressive strength of LSG mortar cubes with and without exposure to acid was tested as per ASTM Standard test method C109 [42]. The compressive strengths and residual strength of LSG geopolymer specimens were conducted for all four classifications of geopolymer specimens including a) Na-based LSG specimens exposed to HCl, b) K-based LSG exposed to HCl, c) Na-based LSG exposed to H_2SO_4

Table 2
Mix proportions of LSG containing sodium and potassium based alkaline activators (Note: X denotes alkali such as Na and K; alkaline activator was 50%).

Abbreviations	Lithium Slag (kg/m^3)	Sand	Silica Fume (kg/m^3)	X-Hydroxide (kg/m^3)	X-Silicate (kg/m^3)	Borax (3%)	SiO_2/Al_2O_3
Na-alkaline activators							
$100LS0SF_{Na}$	916.24	916.24	0	114.53	343.59	27.48	2.62
$90LS10SF_{Na}$	824.61	916.24	91.62	114.53	343.59	27.48	3.16
$80LS20SF_{Na}$	740.16	916.24	176.08	114.53	343.59	27.48	3.70
$70LS30SF_{Na}$	643.35	916.24	273.65	114.53	343.59	27.48	4.55
$60LS40SF_{Na}$	556.45	916.24	359.78	114.53	343.59	27.48	5.55
K-alkaline activator							
$100LS0SF_{K}$	916.24	916.24	0	114.53	343.59	27.48	2.62
$90LS10SF_{K}$	824.61	916.24	91.62	114.53	343.59	27.48	3.18
$80LS20SF_{K}$	740.16	916.24	176.08	114.53	343.59	27.48	3.70
$70LS30SF_{K}$	643.35	916.24	273.65	114.53	343.59	27.48	4.55
$60LS40SF_{K}$	556.45	916.24	359.78	114.53	343.59	27.48	5.55

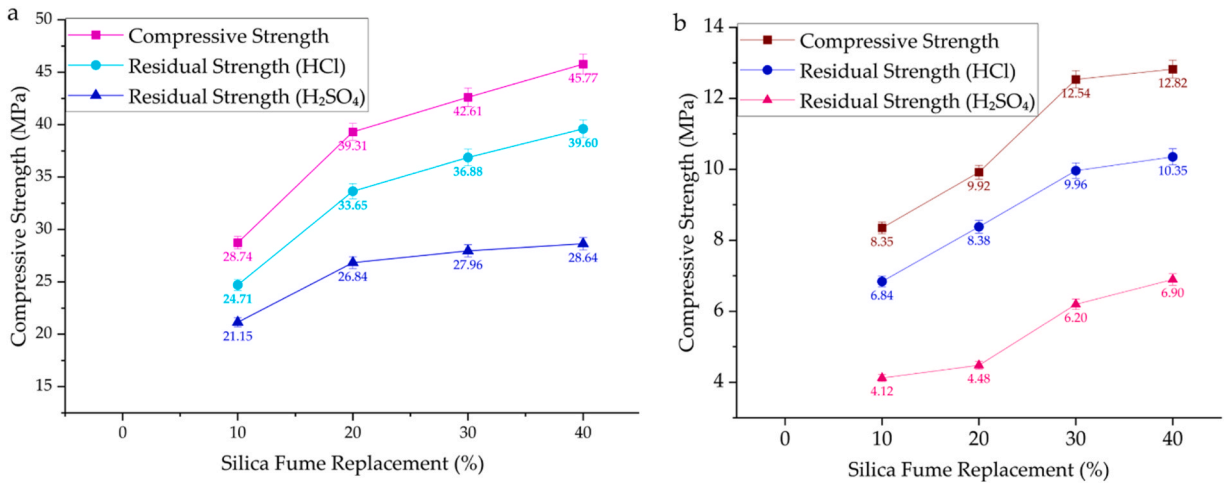

Fig. 3. Compressive strength and residual compressive strength of LSG after acid exposure a) Na-based mixes b) K-based mixes.

and d) K-based LSG exposed to H_2SO_4 acidic solution. The comparative analysis was performed based on residual strength and weight loss after exposure to acid solutions. Alkali activated material containing Na-based alkaline activator were preserved for further microstructural analysis.

2.5.3. *Microstructural investigation*

The microstructural forensic analysis of LSG specimens after exposure to an acidic environment was conducted by SEM/EDS to identify the morphological and chemical changes in the microstructure that may have contributed toward the strength reduction. The acid-exposed specimens of a better-performing set of mixes of sodium-based alkaline activators were selected and 8×8x5 mm^3 chips specimens were prepared. The specimens were coated with 20 nm carbon layer using Cressington platinum sputter coater (Model 208HR). Thereafter, the specimens were tested for SEM and EDS using field emission SEM (MIRA3). The Secondary electron and backscattered electron micrographs, and EDS mapping were performed for identifying the morphology, and chemical composition of emerging phases and microstructure after acid exposure that may have contributed toward strength degradation.

2.5.4. *Reaction kinetics*

To correlate the acid resistance of LSG mixes containing varying proportions of silica fume with strength development the reaction kinetics were studied using an 8-channel TAM AIR Isothermal calorimeter (TA Instrument, USA). The test was performed confirming ASTM standard test method C1702 [43]. The calorimeter was initially run for 5 h duration to stabilize the chamber temperature at 20°C which was kept closer to the room temperature 23 ± 2°C to minimize background thermal disturbance. The pastes constituents were weighted based on the proportion mentioned in Table 2, mixed externally, and loaded into the calorimeter. The time elapsed between adding the alkaline activator and the paste being loaded into the calorimeter was 2 min. This method of mixing was adopted to avoid recording instantaneous heat evolution during sudden chemical interaction of concentrated alkaline activators with precursor [44].

3. Discussion of results

3.1. *Compressive strength*

The compressive strength of LSG mortar specimens synthesized using sodium and potassium-based alkaline activators are shown in Fig. 3a, b. The 28 days compressive strength of sodium-based LSG containing 0, 10, 20, 30, 40% of silica fume was recorded as 17.27, 28.74, 39.31, 42.61, and 45.77 MPa, whereas for potassium-based alkaline activator, the compressive strength is 7.20, 8.35, 9.92, 12.54, and 12.82 MPa at 0, 10, 20, 30, 40% incorporation of silica fume, respectively. Generally, there is an increasing trend of compressive strength upon additive incorporation of silica fume in LSG mortars due to increasing Si/Al in the aluminosilicate gel. The compressive strength of potassium-activators is lower than that of sodium-activator based LSG mixes. The lower compressive strength of potassium-activator LSG may have been attributed to the lower concentration of potassium ions in potassium silicate solution as indicated by a lower concentration of K_2O (11.20%) concentration than that of sodium counterpart (14.70). The strength development of LSG mortars containing potassium activators is not proportionately lower with the lower concentration of K_2O in alkali solution in comparison with sodium activators. There might be a

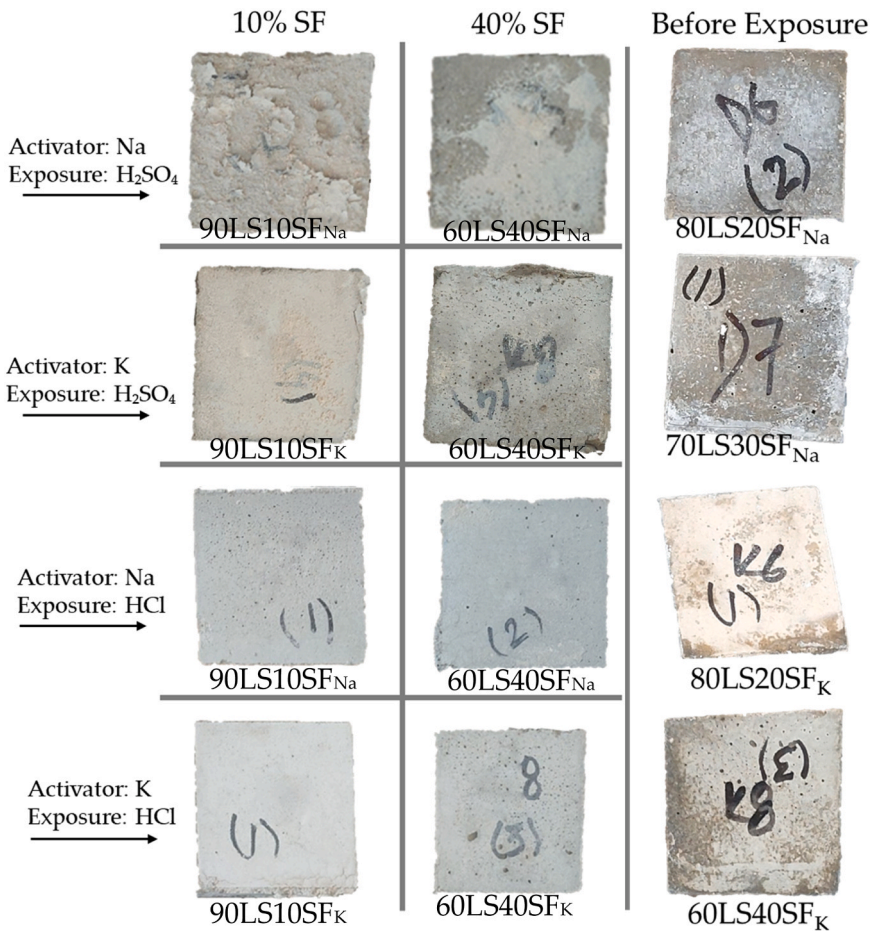

Fig. 5. The deterioration of LSG containing Na and K activators after exposure to H_2SO_4 and HCl (Note: Subscript $_{Na}$ and $_K$ represents the alkaline activator type).

difference in reactivity due to the higher ionic radius and lower charge density of K^+ ions than that of Na^+. Similarly, previous research also reported the lower compressive strength of K-activators fly ash geopolymers containing LSG than that of Na-based geopolymers [45]. Another study investigated the compressive strength of fly ash-based geopolymer for Na and K-based alkaline activators at ambient and elevated temperatures [46]. The compressive strength of potassium-based alkaline activators is lower than Na-based ones. Conclusively, LSG with Na-based activator has higher compressive strength than LSG with K-based alkaline activator.

3.2. Residual compressive strength

The acid exposure of geopolymer composite is one of the accelerated durability analysis pertaining to estimate long-term deterioration in a shorter period [47]. The Fig. 3 shows the acid resistance of LSG samples in terms of residual strength after exposure to 5% H_2SO_4 and HCl solutions. For both sodium and potassium-activator based LSG, the deterioration of the specimens is evident as a decreased residual strength. For specimens exposed to HCl and H_2SO_4, the average percentage drop in compressive strength of the Na-activator was 13.77% and 32.48%, whereas, for K-activator LSG, the average percentage drop in compressive strength was 18.35% and 51.42%, respectively. The specimens exposed to HCl had a higher residual strength than the specimens exposed to H_2SO_4 solution. Both sodium-activator and potassium-activator geopolymers followed similar trends. In cement concrete and geopolymer, H_2SO_4 is thought to deteriorate microstructure greater than HCl due to expansion caused by sulphatic species [48,49]. Similarly, the higher deterioration was caused in the case of H_2SO_4, which may have induced SO_4^{-2} ion migration in the LSG specimens. As a result, it appeared that H_2SO_4 deterioration was greater than HCl deterioration.

The acid deterioration of LSG is represented by weight loss. The weight loss of the LSG_{Na} specimens that were exposed to H_2SO_4 and HCl solutions was 11.85, 10.03, 8.79, 8.75 and 9.54, 7.56, 6.59, 6.39, respectively. For LSG_K specimens, the weight loss for H_2SO_4 and HCl solutions were 18.47, 14.20, 9.96, 7.78 and 12.92, 9.94, 7.11, 5.09, respectively. The deterioration of LSG_{Na} and LSG_K is presented in Fig. 5. The control LSG specimens experienced higher deterioration upon exposure to both HCl and H_2SO_4 solutions, subsequently underwent extensive disintegration. The specimens that were exposed to sulfuric acid experienced higher deterioration in terms of scaling and mineral leaching from aluminosilicate gel, whereas the specimens exposed to HCl only underwent deterioration by leaching marked by decolorization. Moreover, the incorporation of silica fume increased the resistance to the deterioration. The scaling is more pronounced upon exposure of the $90LS10SF_{Na}$ mix to H_2SO_4 solution; however, the minimum scaling was observed in the $60LS40SF_{Na}$ mix, along with fewer white residue. The K-based geopolymer presented no evidence of scaling, but leaching is observed, represented by the decolourization of specimens to a lighter colour.

The specimens after exposure to HCl and H_2SO_4 lost the intrinsic texture and surface appearance due to leaching and deposition of gypsum [50,51]. The silica fume incorporated LSG_{Na} specimens showed increased degradation when exposed to sulphuric acid. This degradation was characterised by weight loss and the formation of more salts on the surface. The precipitation of salts is more pronounced in alkaline activators based on sodium compared to those based on potassium.

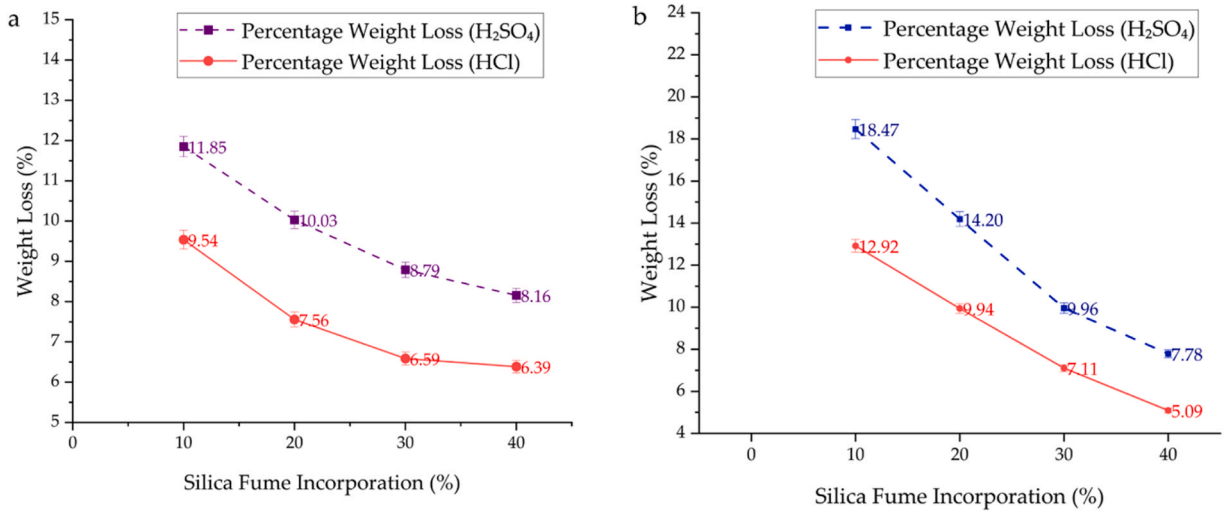

Fig. 4. Weight loss by post-acid exposure of silica fume incorporated LSG containing a) Na-based alkaline activator b) K-based activator.

Additionally, the overall weight loss of LSG_K specimens is greater than that of LSG_{Na} counterparts. Similar trends were observed when both Na and K based geopolymers were exposed to HCl. Therefore, the deterioration of LSG_{Na} and LSG_K exposed to H_2SO_4 solution revealed higher weight loss than the specimens exposed to HCl solution. Fig. 4.

3.3. Calorimetric analysis

3.3.1. Reaction kinetics

The reaction kinetics of the mixes performed well in acid exposure and control LSG are shown in Fig. 6. An exothermic peak is observed during the initial stage of geopolymerization (first 30 min). The exothermic reaction observed can be attributed to the wetting and dissolution process of the aluminosilicate precursor [52]. Early age geopolymerization demonstrates a rapid exothermic response, resembling the induction period witnessed during cement hydration. However, it is important to note that there are distinct variations in the physicochemical reactions between these two processes [53,54].

The initial peak indicates a higher degree of adsorption of the alkali solution and the subsequent breaking of Si-O and Al-O bonds by OH^- anions [55]. The exothermic dissolution of lithium slag particles occurs in an alkaline solution, resulting in the breakdown of Si-O and Al-O bonds on the surfaces of the precursor particles. The initial peak in the wetting process experiences a rapid decline, resulting in a slowdown of both the wetting process and initial reactions, thereafter the reactions continue to generate heat. The observed deceleration curve is attributed to the reorganisation of monomers and the formation of a long-chained aluminosilicate gel [56,57].

During the final stage, the process of nucleation, growth, and precipitation of reaction products occurred within a time frame of four to 15 h. This period signifies the condensation reaction between silicate and aluminate monomers, resulting in the formation of alkali aluminosilicate gels which is also evident in the literature [58]. During this period, it was observed that there was a high amount of heat release and a second peak in the heat release rate. It is important to observe that the second peaks of the control LSG samples is broader compared to the first intense peak. The heat release observed at 1.5 h during the second peak is believed to be caused by the reaction between calcium species (specifically gypsum, calcite) and silicate and aluminate species [59]. This reaction results in the formation of a disintegrated aluminosilicate gel, which has been previously reported in the authors' earlier study [33]. The disappearance of the second peak in the LSG geopolymer-incorporated silica fume, can be attributed to the higher Si/Al ratio and the suppression of the reaction of calcium-bearing minerals with aluminosilicate gel. The exothermic peak observed in control LSG is notably greater in magnitude compared to LSG samples containing 40% silica fume. The observed phenomenon may be attributed to the increased dissolution rate of aluminates, which is characterized by a lower Si/Al ratio. Hence, the inclusion of silica fume has resulted in an increased Si/Al ratio and a steady rate of geopolymerization.

3.3.2. Heat evolution

The integrated individual area of the calorimetric curves shown in Fig. 7a is indicative of the heat released by the one gram of mix in a certain duration of time during various stages of geopolymerization. The reaction kinetics are divided into two reaction regimes, which are the first 5 h and later rest of the curves. The calorimetric curve of LSG without incorporation of silica fume appears to have a higher rate of heat evolution within the first five hours of geopolymerization than LSG mix containing silica fume. The cumulative heat release for curve-II is 676.33 J /g which is quite higher than the heat evolution associated with curve-I (197.86 J/g) as shown in Table 3. The slope within the duration of the first regime of the control LSG mix is around five times higher than the LSG mix containing silica fume. The enormous amount of heat evolved during a short period and thus the abrupt strength development could have caused higher micro-cracking due to thermal shrinkage in the control LSG geopolymer, whereas the incorporation of silica fume stabilizes the reaction kinetics of LSG. The rapid increase in strength can also be observed in Fig. 7a, which illustrates the degree of reactivity over time. In the case of the control LSG mix, 70% of the reaction was completed within the first 1.5 h. On the other hand, in the mix containing 40% of silica fume, only 25% of the reaction was completed within the same duration. In a study conducted by Niu et al. [60], the impact of including sulphatic tailings in alkali activated blast furnace slag was examined. Isothermal calorimetric results revealed that higher inclusion of sulfidic mine tailing with higher sulfate content led to a higher heat evolution at the initial peak and relatively lower strength development. The accelerated geopolymerization during the initial phase of the process results in a decrease in the strength of the composite material. While the initial strength development within the first 1.5 h was comparatively lower in the silica fume incorporated LSG, it exhibited higher strength development in the later stage compared to the control LSG and silica fume incorporation effectively counteracts the adverse impact of thermal cracking. Thus, the strength development was higher in silica fume incorporated geopolymer. Similarly, literature suggested that the strength reduction can be a result of the rapid strength gain during the first 28 days of curing, causing shrinkage and

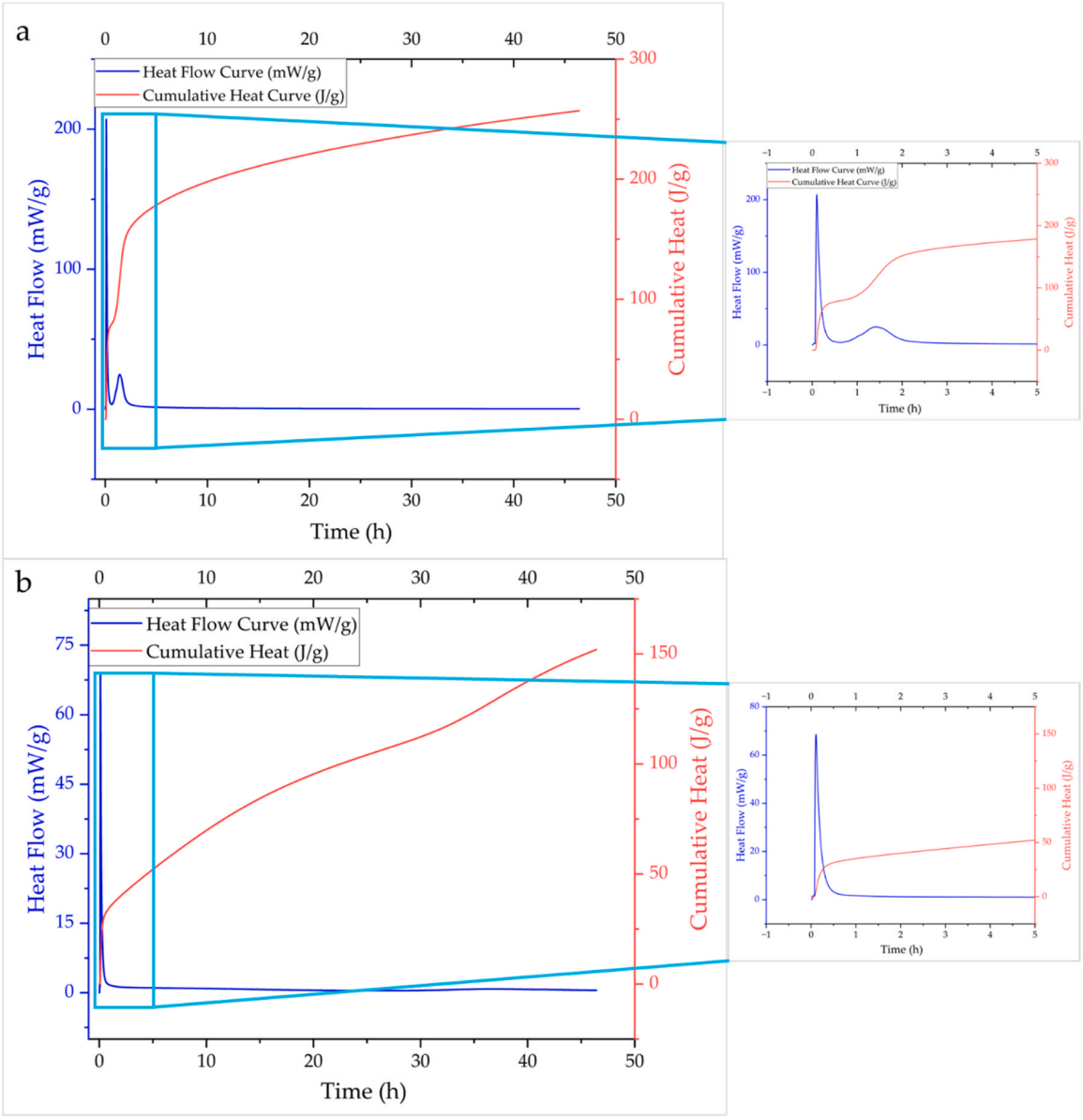

Fig. 6. Heat flow and cumulative heat of geopolymer a) 100LS0SF b) 60LS40SF.

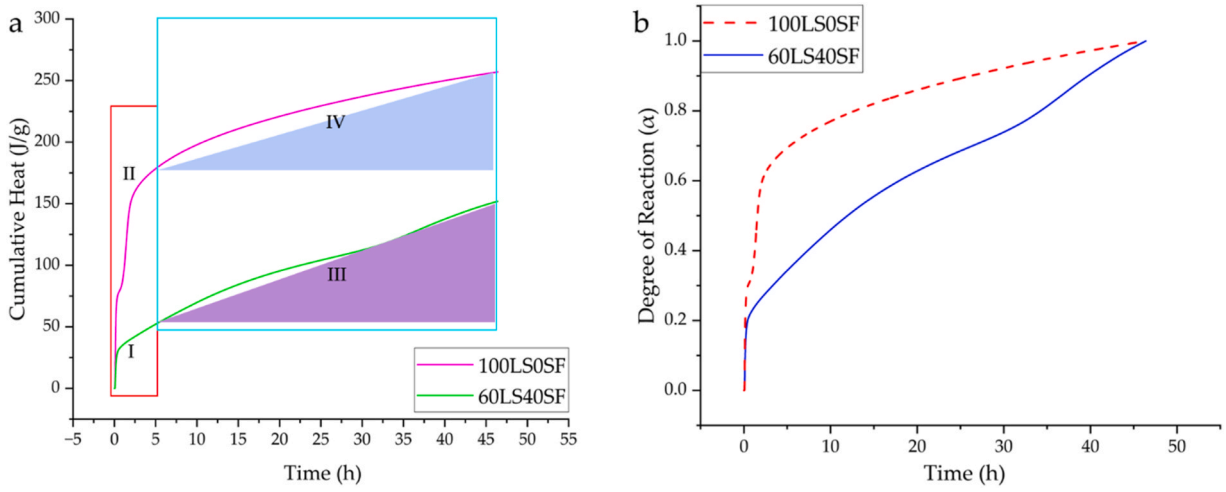

Fig. 7. Cumulative heat evolution at a) stages of geopolymerization b) degree of reactivity of geopolymer composite containing silica fume.

Table 3
Integrated area under the calorimetric curve (*, **Contribution of integrated area under the individual reaction regime).

Calorimetric Curves	Time (hour)	Slope (m)	Integrated area under the curve (J. h/g)
I	0-5	5.77	197.86
II		26.78	676.33
III	5-45	2.23	4360.67-2387.96 = *2344.29
IV		1.73	9403.89-8224.77 = **1179.12

porosity/cracks [61]. The accelerated strength development of LSG at the early-stage results in the formation of cracks and poor microstructure. This, in turn, leads to increased acid penetration within the microstructure, resulting in higher levels of deterioration. The addition of silica fume in LSG resulted in a decrease in the high initial strength development within 3 h, while the strength development over time increased. This is evident from the higher heat of geopolymerization, represented by the area under the curve III. High early heat evolution as a result of geopolymerization affects the microstructure development and overall strength gain. Chen et al. investigated the use of few of the accelerators including $LiCO_3$ as accelerator in geopolymer and observed a prominent decrease in compressive strength above 0.4% of $LiCO_3$ [62]. Hence, the durability performance of silica fume incorporated LSG is also affected by its initial strength gain determined by calorimetry.

3.4. Microstructural investigation

The deterioration of sodium-activator LSG specimens exposed to both H_2SO_4 and HCl is depicted in SEM/EDS micrographs shown in Fig. 8. The SEM micrographs in Fig. 8(b, d, f, h) are the BSE images for identifying the microstructure of the LSG exposed to HCl and H_2SO_4 along with the EDS spectra. The lithium slag geopolymer containing silica fume exposed to HCl and H_2SO_4 are shown in Fig. 8(a-d), and (e-h), respectively. The spectral peaks are shown on the EDS spectra gives insight about the chemical composition after microstructural degradation.

The formation of calcium sulphate needle shaped crystals was observed upon the exposure of geopolymer specimens to H_2SO_4 and there was no major corrosion appeared within the microstructure of specimens exposed to HCl that could have caused the major strength degradation. The main similarity between both types of acidic environments is the leaching of Al ions as their EDS peak vanished or reduced significantly. The LSG specimens exposed to H_2SO_4 experienced the formation of clustered crystalline needles containing Ca, S, and O elements forming gypsum/anhydrite, whereas there was no prominent chemical transformation evident from SEM/EDS micrographs for the specimens exposed to HCl solution. Upon exposure to H_2SO_4, the diffuse-ability of HSO^{4-} ions in the microstructure and the recrystallization of gypsum occurred, thus deteriorating the aluminosilicate gel matrix.

The LSG containing 20% silica fume revealed more exposed fine aggregate particles after leaching the aluminosilicate gel and containing cracks, whereas 40% silica fume incorporation LSG significantly improved its acid resistance, and aluminosilicate gel was found encapsulating aggregate. The main deterioration mechanism is governed by the leaching of aluminates and attached alkali cations that damage the N-(C)-A-S-H gel. Moreover, the morphology of LSG exposed to H_2SO_4 resulted in the varied-sized needles of anhydrite. The anhydrite needle was sized around 20 μm and thick between 250–500 nm for the mix containing 20% silica fume, whereas the thickness of anhydrite needles varied between 1–2 μm for 40% silica fume incorporated LSG.

When LSG specimens were immersed in HCl solution, a substitution/leaching process occurred where the Na and Ca ions in the matrix were replaced by H^+ and H_3O^+ ions. This substitution was caused by a variation in pH [63]. Similarly, Ismail et al. [64] examined the resistance of fly ash/slag geopolymer to sulfate and observed that the presence of H^+ ions had a detrimental effect on the aluminosilicate gel. The weakening of intercrystallite bond strength is considered to be the cause of both the disintegration of microstructure and the significant loss of strength in geopolymer materials, as reported by Bakharev [65]. The removal of aluminium ions from the aluminosilicate network gel occurred, resulting in their replacement by silicon atoms. The microstructure exhibited a reduction in aluminium content due to the development of a highly siliceous composition [66].

The acid exposure for both sulphuric acid and hydrochloric acid of LSG-containing silica fume at lower magnifications is shown in Fig. 8a, b and c, d, respectively. The spread of anhydrite throughout the microstructure of LSG exposed to H_2SO_4 could have resulted in the leaching of Ca^+ and SO_4^{-2} components and recrystallized into anhydrite upon variation of pH leaving cracking within the aluminosilicate geopolymer matrix. The cracking observed in backscattered micrographs depicts the cracking by the leaching and disintegration of aluminosilicates and weakening of the interfacial region. These crystals appeared on the aluminosilicate gel endorses the leaching phenomenon and crystallization of gypsum (Fig. 9a). Moreover, the crystallization of calcium sulphate is widely spread over the microstructure revealing the overall representation of leaching at lower resolution. The crystallization of calcium sulphate along with the higher cracking in the microstructure of H_2SO_4 exposed specimens is indicative of higher microstructural deterioration as shown in Fig. 9(a, b). The acid leaching causes cracking and the development of nascent gypsum crystals to the structure of ice flake crystals in an entrapped air bubble which is shown in Fig. 10 (a, b). The flake like formation of calcium sulfate salt crystal by leaching through the aluminosilicate gel further increase the microstructural permeability for future ingress of leaching inhibitors, thus increasing corrosion. Contrarily, LSG exposed to HCl did not undergo any apparent morphological or chemical transformation aside from leaching of Al and subsequently inducing porosity in aluminosilicate gel. On the other hand, the LSG exposed to H_2SO_4 underwent higher degradation than HCl.

The EDS-mapped micrographs of the 20% incorporated LSG geopolymer exposed to HCl solution at higher and lower magnification is shown in Fig. 10a and b, respectively. The crystals of gypsum are shown in a mapped SEM micrograph, the colour of their spectra ranges from greenish to dark orange which refers to lower and higher spectral values of Ca, respectively. The distribution of gypsum throughout the microstructure is evident from spectral micrographs (Fig. 10b). The coexistence of Al and Si on spectral micrographs in aluminosilicate gel is a widely accepted fact, whereas the phenomenal leaching of Al from aluminosilicate gel is indicated by separated Si and Al spectra in the micrographs (Fig. 10b). The cyan colour in EDS spectra represents the leached Al which widely exists in aluminosilicate gel microstructure marked by the blend of Si and Al spectra. The microstructural deterioration upon exposure to HCl resulted in leaching and the formation of gypsum/anhydrite needle-shaped crystals by leaching of Ca^+ and SO_4^{-2} ions upon variation of pH leaving cracks. The leaching of Al from the microstructure is also evident from EDS spectral map deteriorating the aluminosilicate gel structure. Similarly, a published study reported the leaching of Na and Al elements from fly ash geopolymer when exposed to 10% sulphuric acid deleteriously damaging aluminosilicate gel [67]. Yang et al. [68] reported the formation of gypsum in geopolymer upon exposure to an acidic environment due to the presence of calcite in geopolymer paste matrix.

The sulphate attack mechanism in LSG are described as follows:

1. Ion exchange occurs, causing sodium to migrate into the acid solution, whereas H+ , H_3O+ , and SO_4^{-2} ions transfer into the samples.
2. Simultaneously, protons and hydronium ions (H^+, H_3O^+) attack the Si-O-Al bonds, resulting in the expulsion of aluminium into the acid solution and the formation of a siliceous framework [51,69].
3. Along with sodium and aluminium, trace amounts of calcium, potassium, magnesium, and iron are also present in the acid solution.

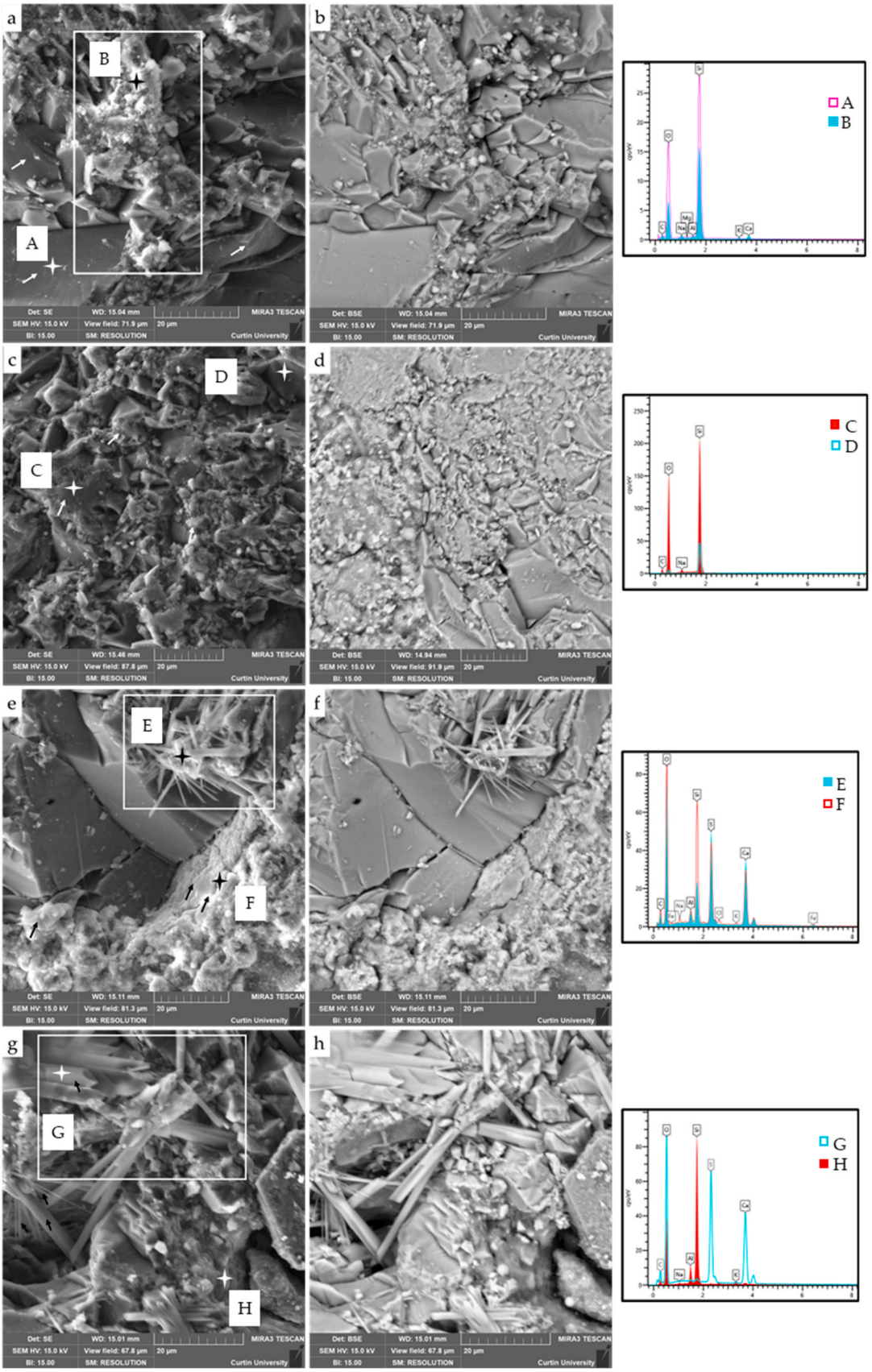

Fig. 8. Micromorphology of LSG containing sodium-activator solution a, b) 80LS20SF$_H$; c, d) 60LS40SF$_H$; e, f) 80LS20SF$_S$; g, h) 60LS40SF$_S$ (Note: Subscript 's' represents exposure to H_2SO_4, and subscript '$_H$' represents exposure to HCl).

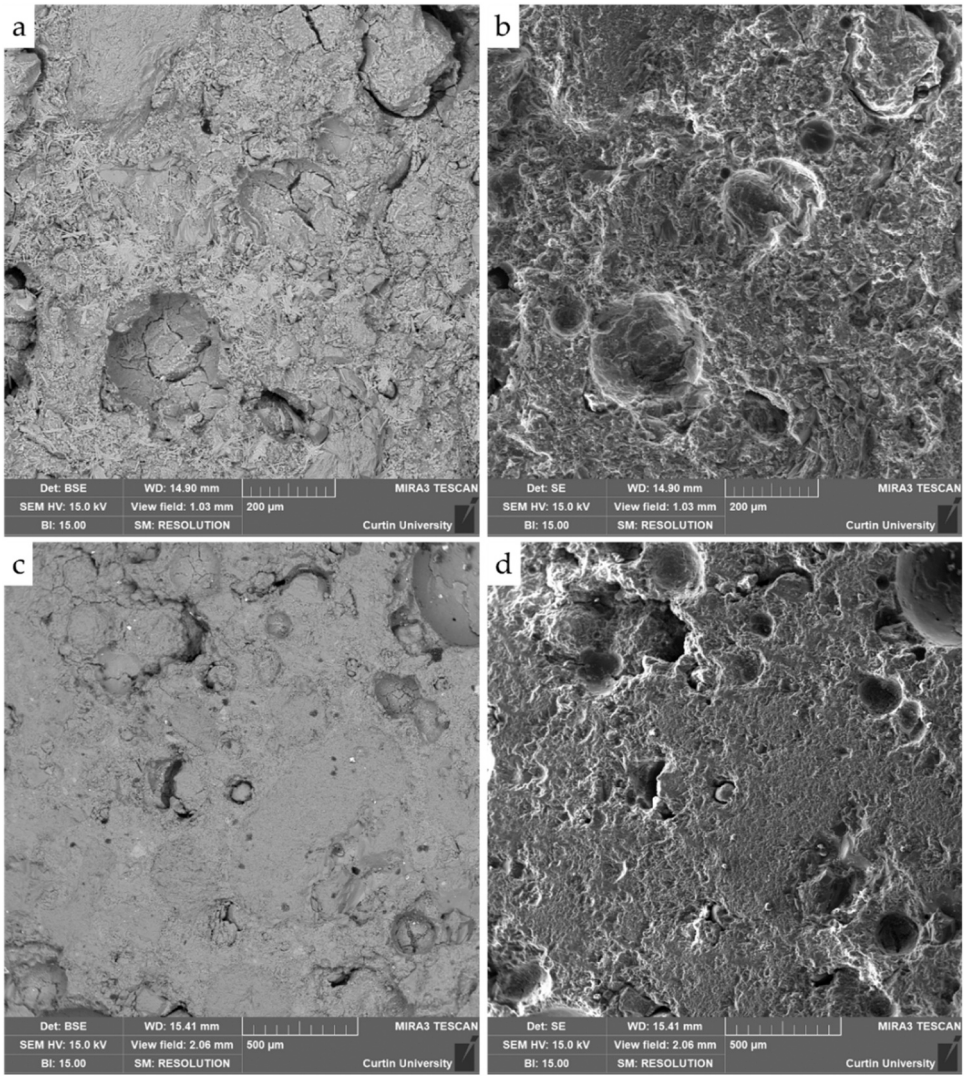

Fig. 9. Generation of calcium sulfate crystals and cracking of LSG containing sodium activators upon acid exposure a, b) 60LS40SF$_{\mathbf{S}}$; c, d) 60LS40SF$_{\mathbf{H}}$ (Note: 's' represents exposure to H_2SO_4, and '$_H$' represents exposure to HCl).

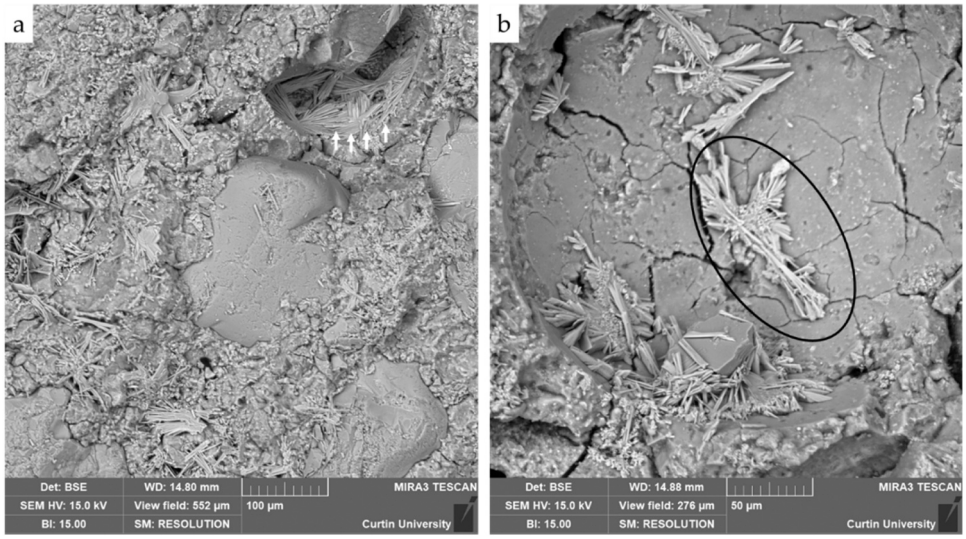

Fig. 10. Micro-cracking of microstructure after crystallization of calcium sulfate in 60LS40SF$_{\mathbf{S}}$ mix at various magnification (Note: Subscript 's' represents exposure to H_2SO_4).

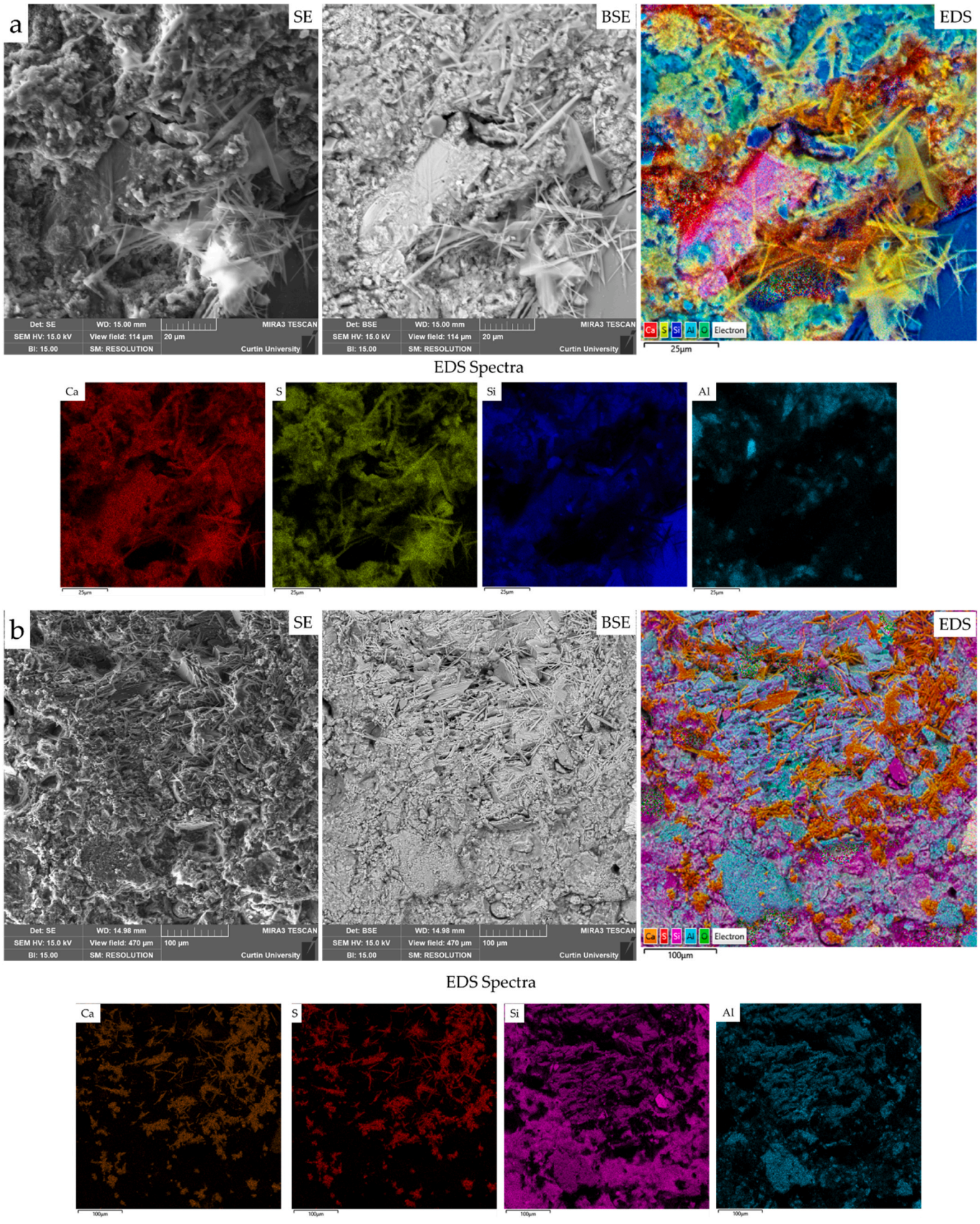

Fig. 11. EDS mapped micrographs of 80LS20SF$_s$ at a) higher magnification, b) lower magnification (Note: 's' represents exposure to H_2SO_4).

4. When diffusing SO_4^{-2} anions collide with counter-diffusing calcium ions, gypsum crystals form within the penetrated layer. The amount of gypsum formed increases as lithium slag is in higher concentration. This gypsum deposition has a negative impact on the material, generating cracks and eventually leading to significant fractures, thus expose the microstructure for further ingress of corrosion inhibitors [50].

In conclusion, the LSG geopolymer's EDS-mapped micrographs after exposure to HCl and H_2SO_4 reveal deep insight into the microstructure degradation. Ion exchange, Si-O-Al bond breakdown, and gypsum crystal formation cause structural deterioration and corrosion upon H_2SO_4 exposure. Whereas the HCl exposure results into the leaching of Al ions along with induced porosity of the microstructure. Fig. 11.

4. Conclusions

This research investigated the accelerated deterioration of silica fume incorporated LSG mortars by their exposure to a strong acidic environment. The deterioration was measured in terms of residual strength and weight loss, whereas the highly acid-resistant mixes were further investigated for micro-forensic analysis and strength development by reaction kinetics. The brief conclusions are presented below.

1. The compressive strength of LSG mortars increased with the increase of silica fume content for both geopolymer mortars using sodium and potassium activators. A higher compressive strength was observed for sodium-activator geopolymer due to having a higher content of alkali cations in it. The maximum compressive strength value of 45.77 MPa was found in the LSG mortar mix with 40% silica fume.
2. The residual compressive strength of LSG mortar specimens after being exposed to 5% H_2SO_4 and HCl separately. The deterioration of specimens exposed to H_2SO_4 was higher than the specimens exposed to HCl. The resistances to strength degradation and corrosion of sodium-activator LSG mortars were higher than those of potassium-activator counterparts. The maximum residual compressive strengths of 39.60 and 28.64 MPa were observed for 40% silica fume incorporated LSG mortars exposed to HCl and H_2SO_4, respectively.
3. The reaction kinetics of LSG incorporating silica fume resulted in a steady evolution of heat during the early dissolution of aluminosilicate and the overall strength development in terms of heat evolution was almost double than that of the control LSG. The second calorimetric peak in control LSG represents the crystallization of calcium silicate during polycondensation of aluminate and silicate monomers. The higher initially evolved heat of geopolymerization and crystallization of anhydrite may have induced disintegration in aluminosilicate gel.
4. The strength development of LSG geopolymer is governed by the cumulative heat release between 5 to 48 h of geopolymerization. The higher slope (2.23) of the cumulative heat curve of LSG containing 40% silica fume is indicative of a higher degree geopolymerization and enhanced microstructure, whereas control LSG resulted in lower degree of geopolymerization marked by a lower slope value (1.73). Hence, the higher formation of aluminosilicate gel in silica fume incorporated gel, consequently denser microstructure is the compelling reason for lower strength degradation upon exposure to acid environments.
5. The deterioration due to acid exposure revealed by microstructural analysis depicted the formation of needle-like calcium sulfate (gypsum) crystals and leaching of Al due to aggressive exposure of H_2SO_4, whereas for LSG after exposure to HCl solution caused the degradation of aluminosilicate gel by only leaching of Al which is evident in EDS spectrum. Hence, the deterioration of aluminosilicate gel by leaching of Al and Ca, Na cations from aluminosilicate gel deteriorates the microstructure of LSG geopolymer.

CRediT authorship contribution statement

Usman Javed: Conceptualization, Data curation, Formal analysis, Investigation, Methodology, Visualization, Writing-original draft, Writing-review & editing. **Faiz Uddin Ahmed Shaikh**: Conceptualization, Funding acquisition, Project administration, Resources, Validation, Supervision, Writing-review & editing. **Prabir Kumar Sarker**: Supervision, Validation, Resources, Writing-review & editing..

Declaration of Competing Interest

The authors declare that they have no known competing financial interests or personal relationships that could have appeared to influence the work reported in this paper.

Data Availability

Data will be made available on request.

Acknowledgment

The authors acknowledge to Australian Research Council (ARC) for providing financial support in this research in the form of Discovery Project grant DP200102784.

References

[1] J.G. Olivier, J.A. Peters, G. Janssens-Maenhout, Trends in global CO2 emissions. 2012 report, (2012).
[2] C.A. Hendriks, E. Worrell, D. De Jager, K. Blok, P. Riemer, Emission reduction of greenhouse gases from the cement industry, Proceedings of the fourth international conference on greenhouse gas control technologies, Interlaken, Austria, IEA GHG R&D Programme, 1998, pp. 939–944.
[3] R.A. Feely, C.L. Sabine, K. Lee, W. Berelson, J. Kleypas, V.J. Fabry, F.J. Millero, Impact of anthropogenic CO_2 on the CaCO3 system in the oceans, Science 305 (5682) (2004) 362–366.
[4] C.L. Sabine, R.A. Feely, N. Gruber, R.M. Key, K. Lee, J.L. Bullister, R. Wanninkhof, C. Wong, D.W. Wallace, B. Tilbrook, The oceanic sink for anthropogenic CO_2, science 305 (5682) (2004) 367–371.
[5] F. Puertas, B. González-Fonteboa, I. González-Taboada, M. Alonso, M. Torres-Carrasco, G. Rojo, F. Martínez-Abella, Alkali-activated slag concrete: Fresh and hardened behaviour, Cem. Concr. Compos. 85 (2018) 22–31.
[6] J.L. Provis, J.S. Van Deventer, Alkali Activated Materials: State-of-the-art Report. RILEM TC 224-AAM, Springer Science & Business Media, 2013.
[7] J.S.J. van Deventer, J.L. Provis, P. Duxson, G.C. Lukey, Reaction mechanisms in the geopolymeric conversion of inorganic waste to useful products, J. Hazard. Mater. 139 (3) (2007) 506–513.
[8] P. Duxson, A. Fernandez-Jimenez, J.L. Provis, G.C. Lukey, A. Palomo, J.S.J. van Deventer, Geopolymer technology: the current state of the art, J. Mater. Sci. 42 (9) (2007) 2917–2933.
[9] X.Y. Zhuang, L. Chen, S. Komarneni, C.H. Zhou, D.S. Tong, H.M. Yang, W.H. Yu, H. Wang, Fly ash-based geopolymer: clean production, properties and applications, J. Clean. Prod. 125 (2016) 253–267.
[10] P. Rovnanik, Effect of curing temperature on the development of hard structure of metakaolin-based geopolymer, Constr. Build. Mater. 24 (7) (2010) 1176–1183.
[11] T.W. Cheng, J.P. Chiu, Fire-resistant geopolymer produced by granulated blast furnace slag, Miner. Eng. 16 (3) (2003) 205–210.
[12] J.C. Kuri, S. Majhi, P.K. Sarker, A. Mukherjee, Microstructural and non-destructive investigation of the effect of high temperature exposure on ground ferronickel slag blended fly ash geopolymer mortars, J. Build. Eng. 43 (2021).
[13] P. Duxson, J.L. Provis, Designing precursors for geopolymer cements, J. Am. Ceram. Soc. 91 (12) (2008) 3864–3869.
[14] L.T. Peiro, G.V. Mendez, R.U. Ayres, Lithium: sources, production, uses, and recovery outlook, Jom 65 (8) (2013) 986–996.
[15] Z.L. Hu, M. Wyrzykowski, P. Lura, Estimation of reaction kinetics of geopolymers at early ages, Cem. Concr. Res. 129 (2020).
[16] G. De Schutter, L. Taerwe, General hydration model for portland-cement and blast-furnace slag cement, Cem. Concr. Res. 25 (3) (1995) 593–604.
[17] X. Zhou, Y.C. Chen, S.X. Dong, H.H. Li, Geopolymerization kinetics of steel slag activated gasification coal fly ash: a case study for amorphous-rich slags, J. Clean. Prod. 379 (2022).
[18] S.K. Nath, S. Mukherjee, S. Maitra, S. Kumar, Kinetics study of geopolymerization of fly ash using isothermal conduction calorimetry, J. Therm. Anal. Calorim. 127 (3) (2017) 1953–1961.
[19] Geopolymers: Structure, Processing, Properties and Industrial Applications, Woodhead Publ Mater (2009) 1–454.
[20] Y. Senhadji, H. Siad, G. Escadeillas, A.S. Benosman, R. Chihaoui, M. Mouli, M. Lachemi, Physical, mechanical and thermal properties of lightweight composite

mortars containing recycled polyvinyl chloride, Constr. Build. Mater. 195 (2019) 198–207.
[21] K. Arbi, M. Nedeljkovic, Y.B. Zuo, G. Ye, A review on the durability of alkali-activated fly ash/slag systems: advances, issues, and perspectives, Ind. Eng. Chem. Res. 55 (19) (2016) 5439–5453.
[22] M.M. Hossain, M.R. Karim, M.K. Hossain, M.N. Islam, M.F.M. Zain, Durability of mortar and concrete containing alkali-activated binder with pozzolans: a review, Constr. Build. Mater. 93 (2015) 95–109.
[23] F.U. Shaikh, Effects of alkali solutions on corrosion durability of geopolymer concrete, Adv. Concr. Constr. 2 (2) (2014) 109.
[24] M. Wasim, T.D. Ngo, D. Law, A state-of-the-art review on the durability of geopolymer concrete for sustainable structures and infrastructure, Constr. Build. Mater. 291 (2021), 123381.
[25] M. Alexander, A. Bertron, N. De Belie, Performance of Cement-based Materials in Aggressive Aqueous Environments, Springer, 2013.
[26] M. Santhanam, M.D. Cohen, J. Olek, Sulfate attack research—whither now? Cem. Concr. Res. 31 (6) (2001) 845–851.
[27] F. Bellmann, B. Moser, J. Stark, Influence of sulfate solution concentration on the formation of gypsum in sulfate resistance test specimen, Cem. Concr. Res. 36 (2) (2006) 358–363.
[28] E. Gruyaert, P. Van den Heede, M. Maes, N. De Belie, Investigation of the influence of blast-furnace slag on the resistance of concrete against organic acid or sulphate attack by means of accelerated degradation tests, Cem. Concr. Res. 42 (1) (2012) 173–185.
[29] F. Shaheen, B. Pradhan, Influence of sulfate ion and associated cation type on steel reinforcement corrosion in concrete powder aqueous solution in the presence of chloride ions, Cem. Concr. Res. 91 (2017) 73–86.
[30] F.A. Shilar, S.V. Ganachari, V.B. Patil, T.M.Y. Khan, N.M. Almakayeel, S. Alghamdi, Review on the relationship between nano modifications of geopolymer concrete and their structural characteristics, Polymers 14 (7) (2022).
[31] P. De Silva, K. Sagoe-Crenstil, V. Sirivivatnanon, Kinetics of geopolymerization: role of Al2O3 and SiO2, Cem. Concr. Res. 37 (4) (2007) 512–518.
[32] F.U.A. Shaikh, Mechanical properties of recycled aggregate concrete containing ternary blended cementitious materials, Int. J. Sustain. Built Environ. 6 (2) (2017) 536–543.
[33] U. Javed, F.U.A. Shaikh, P.K. Sarker, Microstructural investigation of lithium slag geopolymer pastes containing silica fume and fly ash as additive chemical modifiers, Cem. Concr. Comp. 134 (2022).
[34] U. Javed, F.U.A. Shaikh, P.K. Sarker, Microstructural investigation of thermo-mechanically processed lithium slag for geopolymer precursor using various characterization techniques, Constr. Build. Mater. 342 (2022).
[35] N.K. Salakjani, P. Singh, A.N. Nikoloski, Acid roasting of spodumene: microwave vs. conventional heating, Miner. Eng. 138 (2019) 161–167.
[36] M.G. Aylmore, K. Merigot, W.D. Rickard, N.J. Evans, B.J. McDonald, E. Catovic, P. Spitalny, Assessment of a spodumene ore by advanced analytical and mass spectrometry techniques to determine its amenability to processing for the extraction of lithium, Miner. Eng. 119 (2018) 137–148.
[37] F.U.A.S. Usman Javed, Prabir Kumar Sarker, A comprehensive micro-nano investigative approach to study the development of aluminosilicate gel in binary blends of lithium slag geopolymer, Cement Concrete Comp (2023).
[38] F.S.Usman Javed, Prabir Sarker, A comprehensive micro-nano investigative approach to study the development of aluminosilicate gel in binary blends of lithium slag geopolymer, Cem. Concr. Comp. (2023).
[39] Z. Liu, J.X. Wang, Q.K. Jiang, G.D. Cheng, L. Li, Y.X. Kang, D.M. Wang, A green route to sustainable alkali-activated materials by heat and chemical activation of lithium slag, J. Clean. Prod. 225 (2019) 1184–1193.
[40] A. C511, Standard specification for mixing rooms, moist cabinets, moist rooms, and water storage tanks used in the testing of hydraulic cements and concretes, ASTM International West Conshohocken PA, 2021.
[41] A. C267, Standard Test Methods for Chemical Resistance of Mortars, Grouts, and Monolithic Surfacings and Polymer Concretes, C267, 2020.
[42] ASTM, Standard test method for compressive strength of hydraulic cement mortars (using 2-in. or [50-mm] cube specimens), Annu. Book ASTM Stand. Annu. Book ASTM Stand. 4 (1) (2013) 1–9.
[43] ASTM, Standard Test Method for Measurement of Heat of Hydration of Hydraulic Cementitious Materials Using Isothermal Conduction Calorimetry, C1702–17, 2017.
[44] R. Abousnina, A. Manalo, W. Lokuge, Z.H. Zhang, Effects of light crude oil contamination on the physical and mechanical properties of geopolymer cement mortar, Cem. Concr. Comp. 90 (2018) 136–149.
[45] F. Shaikh, S. Haque, Effect of nano silica and fine silica sand on compressive strength of sodium and potassium activators synthesised fly ash geopolymer at elevated temperatures, Fire Mater. 42 (3) (2018) 324–335.
[46] A. Hosan, S. Haque, F. Shaikh, Compressive behaviour of sodium and potassium activators synthetized fly ash geopolymer at elevated temperatures: a comparative study, J. Build. Eng. 8 (2016) 123–130.
[47] S.A. Hadigheh, F.H. Ke, H. Fatemi, Durability design criteria for the hybrid carbon fibre reinforced polymer (CFRP)-reinforced geopolymer concrete bridges, Structures 35 (2022) 325–339.
[48] M. Vafaei, A. Allahverdi, P. Dong, N. Bassim, M. Mahinroosta, Resistance of red clay brick waste/phosphorus slag-based geopolymer mortar to acid solutions of mild concentration, J. Build. Eng. 34 (2021).
[49] J. Kwasny, T.A. Aiken, M.N. Soutsos, J.A. McIntosh, D.J. Cleland, Sulfate and acid resistance of lithomarge-based geopolymer mortars, Constr. Build. Mater. 166 (2018) 537–553.
[50] T.A. Aiken, J. Kwasny, W. Sha, M.N. Soutsos, Effect of slag content and activator dosage on the resistance of fly ash geopolymer binders to sulfuric acid attack, Cem. Concr. Res. 111 (2018) 23–40.
[51] A. Allahverdi, F. Skvára, Nitric acid attack on hardened paste of geopolymeric cements -: Part 1, Ceram. -Silik. 45 (3) (2001) 81–88.
[52] C. Shi, D. Roy, P. Krivenko, Alkali-Activated Cements and Concretes, CRC press, 2003.
[53] Z.Q. Sun, A. Vollpracht, Isothermal calorimetry and in-situ XRD study of the NaOH activated fly ash, metakaolin and slag, Cem. Concr. Res. 103 (2018) 110–122.
[54] G.W. Liang, T.J. Liu, H.X. Li, K. Wu, Shrinkage mitigation, strength enhancement and microstructure improvement of alkali-activated slag/fly ash binders by ultrafine waste concrete powder, Compos Part B-Eng. 231 (2022).
[55] X. Yao, Z.H. Zhang, H.J. Zhu, Y. Chen, Geopolymerization process of alkali-metakaolinite characterized by isothermal calorimetry, Thermochim. Acta 493 (1-2) (2009) 49–54.
[56] C. Shi, R.L. Day, Early strength development and hydration of alkali-activated blast furnace slag/fly ash blends, Adv. Cem. Res. 11 (4) (1999) 189–196.
[57] A. Buchwald, H. Hilbig, C. Kaps, Alkali-activated metakaolin-slag blends - performance and structure in dependence of their composition, J. Mater. Sci. 42 (9) (2007) 3024–3032.
[58] J. Aupoil, J.B. Champenois, J.B.D. de Lacaillerie, A. Poulesquen, Interplay between silicate and hydroxide ions during geopolymerization, Cem. Concr. Res. 115 (2019) 426–432.
[59] C.K. Yip, G.C. Lukey, J.L. Provis, J.S.J. van Deventer, Effect of calcium silicate sources on geopolymerisation, Cem. Concr. Res. 38 (4) (2008) 554–564.
[60] H. Niu, J. Helser, I.J. Corfe, J. Kuva, A.R. Butcher, V. Cappuyns, P. Kinnunen, M. Illikainen, Incorporation of bioleached sulfidic mine tailings in one-part alkali-activated blast furnace slag mortar, Constr. Build. Mater. 333 (2022).
[61] T. Luukkonen, H. Sreenivasan, Z. Abdollahnejad, J. Yliniemi, A. Kantola, V. V. Telkki, P. Kinnunen, M. Illikainen, Influence of sodium silicate powder silica modulus for mechanical and chemical properties of dry-mix alkali-activated slag mortar, Constr. Build. Mater. 233 (2020).
[62] T. Chen, B. Ren, Z.H. Wang, X. Meng, Y.P. Ning, Y. Lv, Effect of early strength agent on the hydration of geopolymer mortar at low temperatures, Case Stud. Constr. Mat. 17 (2022).
[63] R.R. Lloyd, J.L. Provis, J.S.J. van Deventer, Acid resistance of inorganic polymer binders. 1. Corrosion rate, Mater. Struct. 45 (1-2) (2012) 1–14.
[64] I. Ismail, S.A. Bernal, J.L. Provis, S. Hamdan, J.S.J. van Deventer, Microstructural changes in alkali activated fly ash/slag geopolymers with sulfate exposure, Mater. Struct. 46 (3) (2013) 361–373.
[65] T. Bakharev, Resistance of geopolymer materials to acid attack, Cem. Concr. Res. 35 (4) (2005) 658–670.
[66] A. Allahverdi, F. Skvara, Sulfuric acid attack on hardened paste of geopolymer cements - part 2. Corrosion mechanism at mild and relatively low concentrations, Ceram. -Silik. 50 (1) (2006) 1–4.
[67] X. Song, M. Marosszeky, M. Brungs, Z.-T. Chang, Response of geopolymer concrete to sulphuric acid attack, Proc. World Congr. Geopolym. (2005) 157–160.
[68] W. Yang, P.H. Zhu, H. Liu, X.J. Wang, W. Ge, M.Q. Hua, Resistance to sulfuric acid corrosion of geopolymer concrete based on different binding materials and alkali concentrations, Materials 14 (23) (2021).
[69] A. Allahverdi, F. Skvára, Nitric acid attack on hardened paste of geopolymeric cements -: Part 2, Ceram. -Silik. 45 (4) (2001) 143–149.